Kim *et al. Energy Mater.* **2025**, *5*, 500071
DOI: 10.20517/energymater.2024.278

Energy Materials

Article

Open Access

Check for updates

Improving silicon anode durability through uniform dispersion and binding enhancement with polyacrylamide-grafted carbon nanotubes

Yeongseok Kim[#], Seoha Nam[#], Yiso Jeon, Jaeho Jung, Dong-Yeob Han, Soojin Park[*]

Department of Chemistry and Department of Battery Engineering, Pohang University of Science and Technology (POSTECH), Pohang 37673, Republic of Korea.
[#]Authors contributed equally.

[*]**Correspondence to:** Prof. Soojin Park, Department of Chemistry, Pohang University of Science and Technology (POSTECH), 77 Cheongam-Ro, Nam-gu, Pohang 37673, Republic of Korea. E-mail: soojin.park@postech.ac.kr

How to cite this article: Kim, Y.; Nam, S.; Jeon, Y.; Jung, J.; Han, D. Y.; Park, S. Improving silicon anode durability through uniform dispersion and binding enhancement with polyacrylamide-grafted carbon nanotubes. *Energy Mater.* **2025**, *5*, 500071. https://dx.doi.org/10.20517/energymater.2024.278

Received: 5 Dec 2024 **First Decision:** 24 Dec 2024 **Revised:** 3 Jan 2025 **Accepted:** 7 Jan 2025 **Published:** 13 Mar 2025

Academic Editor: Bin Wang **Copy Editor:** Ping Zhang **Production Editor:** Ping Zhang

Abstract

Silicon (Si) anodes offer a high specific capacity (> 3,500 mA h g^{-1}), but severe volume changes during cycling and poor intrinsic conductivity hinder commercialization. Carbon nanotubes (CNTs) are commonly incorporated to improve the electronic conductivity of Si electrodes, but their tendency to aggregate in polar solvent-based slurries leads to non-uniform electrodes. To address this, we synthesize polyacrylamide-grafted CNTs (PAM-g-CNTs) by covalently attaching hydrophilic acrylamide monomers to CNT surfaces. The PAM chains provide steric hindrance that minimizes van der Waals interactions between PAM-g-CNTs and interacts effectively with polar solvents, thus promoting uniform dispersion and forming a stable electron-conductive network within the electrode. Furthermore, PAM-g-CNTs establish hydrogen bonds with Si particles and binder matrices, enhancing the structural integrity of the electrode. The cycling performance of Si half cells incorporating PAM-g-CNTs shows substantial durability after 200 cycles. Moreover, in high-energy-density Si electrode configurations with reduced binder and conductive agent ratios (active material > 70%), PAM-g-CNT-based cells preserved 70% of their initial capacity after 100 cycles, compared to only 20% retention in Super P-based cells. The functionalization of CNTs with hydrophilic PAM thus proves effective in improving dispersion stability and conductivity while reinforcing electrode cohesion. This strategy presents a promising path for developing durable Si anodes for high-energy-density lithium-ion batteries.

Keywords: Silicon anode, carbon nanotubes, polymer grafting, uniform dispersion, polymeric binder

INTRODUCTION

Silicon (Si) is a promising anode material for high-energy-density anodes in rechargeable lithium-ion batteries (LIBs), given its high specific capacity (> 3,500 mA h g^{-1}) and low lithiation potential (~0.4 V *vs.* Li/Li^+)[1-3]. However, its commercial application is hindered by a substantial volume expansion of up to 300% during cycling and intrinsically low electronic conductivity[4-6]. Although polymer-based binders have been extensively explored to alleviate Si particle expansion, their non-conductive properties restrict efficient electron transfer throughout the Si anodes[7,8]. Consequently, Si anodes necessitate large amounts of conductive additives, reducing the proportion of active material within the electrode and consequently resulting in energy density losses[9]. Thus, overcoming these limitations is crucial for enabling the practical application of Si anodes in high-energy-density LIBs.

Super P (SP) carbon black, a widely used commercial conductive agent, consists of small spherical particles that form conductive networks within the electrode based on a point-to-point conduction model[10,11]. In this model, electrons must traverse numerous contact points, with each point introducing resistance and thereby diminishing the overall conduction efficiency. Consequently, SP alone is insufficient for achieving optimal conductivity in Si anodes. On the other hand, carbon nanotubes (CNTs) feature an elongated strand-like structure that provides continuous electron transport paths, promoting uninterrupted and efficient electron flow across the electrode[12,13]. The large surface area of CNTs further increases contact with active materials, boosting conductivity even with minimal CNT content[14,15]. Therefore, many studies have used CNTs to create a conductive network on silicon ->Si electrodes, aiming to minimize volume changes, maintain reliable electrical contact, and facilitate efficient electron and Li^+ transport during battery operation[16]. However, incorporating CNTs in Si electrodes faces challenges due to the hydrophobicity of CNT surfaces and pronounced van der Waals interactions arising from their large surface area, which result in aggregation in polar solvent-based Si electrode slurries[17]. As the non-uniform dispersion of CNTs can disrupt ion and electron flow, ensuring the homogeneous distribution of CNTs is imperative to enhance the electrochemical performance of electrodes [Scheme 1].

Several methods have been reported to improve the dispersibility of CNTs. Avilés *et al.* introduced oxygen-containing functional groups onto CNT surfaces through acid treatment, increasing the hydrophilicity of CNTs and promoting stronger interactions with polar solvents, thereby reducing aggregation[18]. However, the use of strong acids can damage the sp^2 hybridization of CNTs, adversely affecting electron transport[19,20]. Zhou *et al.* synthesized Si-CNT composites by growing CNTs on the Si surface via chemical vapor deposition at 850 °C, achieving stable cycling performance for up to 1,200 cycles[21]. Nevertheless, the high operational temperatures (700-1000 °C) required for synthesis limit its commercial feasibility[22-25]. An alternative to this is to utilize polymers in the CNTs to change the properties of the CNTs[26]; polymer grafting has emerged as an effective strategy, enabling surface functionalization at moderate temperatures (60-100 °C) with minimal impact on CNT structural stability[27].

Herein, we synthesized polyacrylamide-grafted CNTs (PAM-g-CNTs) by grafting acrylamide (AAm) onto the CNT surface. The introduction of amide groups offers a strong affinity for water molecules, and hydrogen bonding interactions between aqueous solvents and PAM-g-CNTs promote uniform dispersion in water-based slurries[28]. This homogeneous arrangement of CNT ultimately facilitates an efficient network to transport lithium ions (Li^+) and electrons[29]. Also, PAM-g-CNTs establish a robust binding system through a hydrogen bond between polar functional groups and slurry components. Consequently, the PAM-g-CNT electrode could maintain a stable electrode structure beyond consecutive volume change based on stronger mechanical strength and adhesion of the electrode compared to CNTs. The high diffusivity of ions and electrons and structural integrity had a synergetic effect on the electrochemical

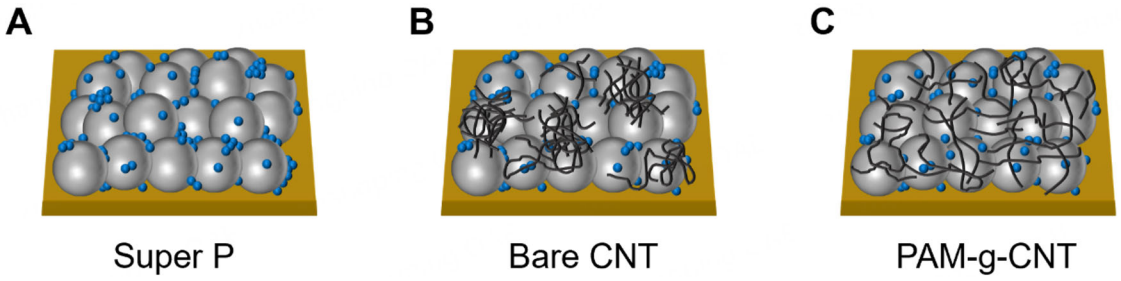

Scheme 1. Schematic illustration of Si anodes with (A) Super P; (B) Super P with CNTs; and (C) Super P with PAM-g-CNTs, emphasizing the uniform dispersion of PAM-g-CNTs within the electrode. CNTs: Carbon nanotubes; PAM-g-CNTs: polyacrylamide-grafted CNTs.

performance of the battery utilizing PAM-g-CNTs. Notably, in electrodes with an elevated active material content of 80% and reduced binder and conductive agent ratios, PAM-g-CNTs demonstrated stable cycling (72.1%) after 100 cycles. In contrast, commercial conductive agents exhibited substantial capacity fading (20.1%). PAM-g-CNTs can efficiently interact with solvent and slurry components through hydrogen bonds, enhancing water affinity and improving the resistance of Si electrodes against swelling. These characteristics of conductive agents realized advanced electrochemical properties, rate performance, long-term cell performance, and electrodes with high energy density.

EXPERIMENTAL

Materials

If there is no notification about purification, the materials were used as received. Ammonium persulfate (APS, 98%), N,N-dimethylformamide (DMF, anhydrous, 99.8%), AAm (99%), N-methyl-2-pyrrolidone (NMP, ACS reagent), SiO_x with particle size of 500-800 nm and polyvinylpyrrolidone (PVP, Mw = 55 k) were purchased from Sigma-Aldrich (St. Louis, USA). Polyacrylic acid (PAA, Mw = 250 k, 25 wt% solution in water) was obtained from Thermofisher Scientific. CNTs were provided by Jaewon Industrial Co., Ltd., and Si active material (30-50 nm, > 97%) from Nanostructured & Amorphous Materials, Inc. Poly(vinylidene fluoride) (PVDF, KF1100, Mn = 168.8 kg mol^{-1}, polydispersity index = 2.94, KUREHA Chem. Ind.) was used as the polymeric binder in the cathode electrode. SP was sourced from Imerys, and graphite (Gr) from POSCO FUTURE M Inc. A cellulose acetate filter (pore size 0.8 μm) was acquired from ADVANTEC (C020A047A). Water was purified using a PURELAB (ELGA LabWater) system before use.

Synthesis of PAM-g-CNT

For the synthesis of PAM-g-CNTs, the amount of CNTs (0.5 g), APS (0.07 g), and AAm (7 g) were fixed to induce a proper degree of grafting reaction on CNTs. The CNTs were pre-dispersed in a DMF and deionized (DI) water co-solvent using a tip sonicator (VC505, Sonics & Materials, Inc.) for 30 min. This dispersion was then transferred to a 3-neck, 250 mL flask and purged with nitrogen gas for one hour to establish an inert environment. APS and AAm were added to the mixture, initiating the grafting reaction, which was carried out at 60 °C in a temperature-controlled oil bath for 24 h. Afterward, the CNTs were filtered through a cellulose acetate filter (0.8 μm pore size) and dried in a vacuum oven at 70 °C for 8 h, resulting in a black powder.

Synthesis of PVP-CNT

To synthesize PVP-CNTs, 20 mg of CNTs and 20 mg of PVP were dispersed in 20 mL of DI water using a bath sonicator (JAC-3010, KODO) for 2 h. The additional dispersion step was performed with a tip sonicator for 30 min to ensure a fully suspended state. The resulting PVP-CNT solution was filtered through a cellulose acetate filter (0.8 μm pore size) and subsequently dried in a vacuum oven at 70 °C for

8 h, yielding a black powder of PVP-CNTs.

Electrode preparation

PAM-g-CNTs were used for the electrodes in a dispersed solution state. They were dispersed in DI water, and the PAA binder was added. The concentration of CNTs in the dispersion was 1 wt%. The slurry-coating method prepared Si, Si/Gr, and SiO_x/Gr blended electrodes. The slurry was cast on Cu foil without further calendaring. The component ratio of Si, Si/Gr and SiO_x/Gr blended electrodes is according to Supplementary Tables 1-4. All electrodes were dried at 110 °C for at least 6 h. The NCM811 cathodes consisted of NCM811 (94 wt%), SP (3 wt%), and PVdF binder (3 wt%).

Material characterizations

Confocal Raman analysis was performed using a WITec alpha 300R spectrophotometer equipped with an Nd: YAG laser (532 nm excitation wavelength). The surface chemistry of PAM-g-CNT was analyzed by X-ray photoelectron spectroscopy (XPS) using a Thermo Scientific K-Alpha system. Thermogravimetric analysis (TGA) was performed using TGA 500 (TA instruments, New Castle) from room temperature to 800 ºC at a heating rate of 10 ºC min^{-1}. The 180º peel-off test was conducted with a tensile strength machine (DA-01, Petrol LAB) at a constant strain rate of 10 mm min^{-1}. Transmission electron microscopy (TEM) with electron energy loss spectroscopy (EELS) for elemental analysis (JEM-2100F, JEOL) was utilized to examine the nanoscale configuration of CNTs under a 200 kV acceleration voltage. Micro-CT imaging was conducted with a Bruker Skyscan1276, and images were analyzed by Bruker Dataviewer software. The three-dimensional (3D) surface morphology of the Si electrode (3 cm × 2 cm region) was analyzed with a 3D laser microscope (VK-X3050, KEYENCE). Surface and interfacial characterization analysis system (SAICAS) measurements (SAICAS EN-EX, Daipla Wintes) provided data on electrode strength. Field-emission scanning electron microscopy (FE-SEM, Hitachi S-4800, Hitachi) was used for structural analysis with an acceleration voltage of 5.0 kV.

Electrochemical characterizations

CR2032 coin cells (Welcos) were used for electrochemical characterization and were assembled in an argon-filled glove box. The electrolyte solution for all cells consisted of 1 M $LiPF_6$ in ethylene carbonate (EC)/ethyl methyl carbonate (EMC)/dimethyl carbonate (DMC) (3:5:2 v/v) with 10 wt% fluoroethylene carbonate (FEC) (Soulbrain), and Celgard 2400 was used as the separator. The galvanostatic battery tests were conducted using a WBCS-3000 battery cycler (Wonatech) at 25 °C. The Si and Si/Gr half cells were tested in the voltage range of 0.005-1.5 V at 0.05 C for a formation cycle and subsequently at 0.5 C within a range of 0.05-1.2 V. A single-sheet pouch cell was fabricated by stacking a one-sided cathode (5.0 cm × 6.0 cm) and an anode (5.4 cm × 6.4 cm), and the pouch full cell was cycled galvanostatically between 4.2 V and 2.7 V, with a formation cycle at 0.05 C and subsequent cycles at 0.3 C. Electrochemical impedance spectroscopy (EIS) measurements were performed over a frequency range of 100 kHz to 0.1 Hz with a 10 mV amplitude (VSP-300, BioLogic). Cyclic voltammetry (CV) measurements were obtained at 0.1 mV s^{-1} from 0.01-1.5 V.

RESULTS AND DISCUSSION

Characterization of PAM-g-CNTs

The synthetic route of PAM-g-CNTs is depicted in Figure 1A and the morphology of pristine CNT was observed by TEM [Supplementary Figure 1]. PAM-g-CNTs are synthesized by grafting AAm onto the anchoring site on the CNT surface via a free radical polymerization process initiated by APS. Sulfate radicals generated by APS attack the CNT surface, forming highly reactive carbon-centered radicals that facilitate the polymerization of AAm, resulting in PAM chains covalently attached to the CNT[30].

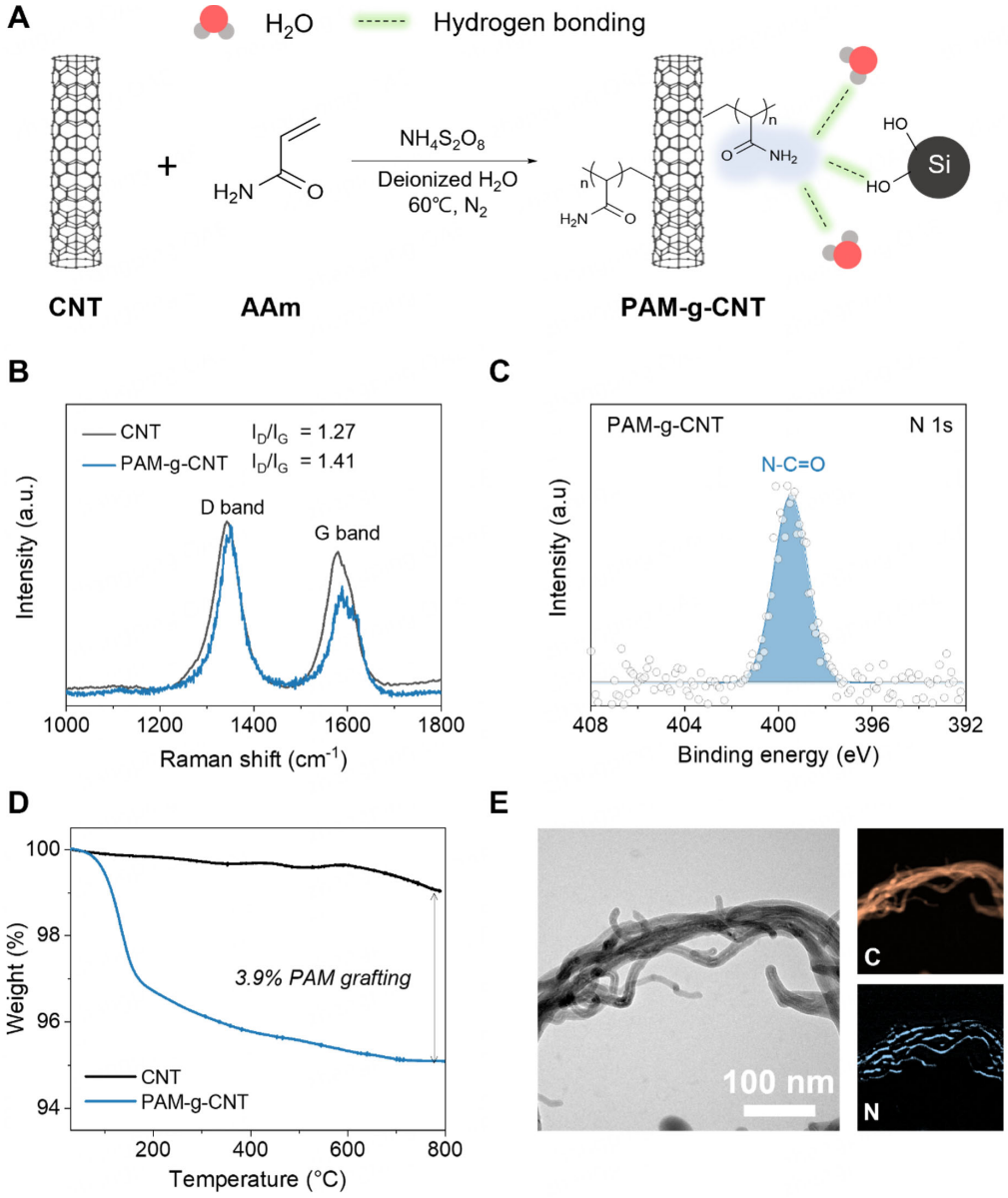

Figure 1. Characterization of PAM-g-CNTs. (A) The scheme showing the synthetic route of PAM-g-CNT; (B) Raman spectra of CNTs and PAM-g-CNTs; (C) N 1s XPS spectra of PAM-g-CNTs; (D) TGA curves of CNTs and PAM-g-CNTs; (E) TEM images and EELS mapping of PAM-g-CNTs. CNTs: Carbon nanotubes; PAM-g-CNTs: polyacrylamide-grafted CNTs; XPS: X-ray photoelectron spectroscopy; TGA: thermogravimetric analysis.

During the grafting process, the formation of carbon-centered radicals on the CNT surface alters the sp^2 hybridization of CNTs to sp^3, creating active sites for AAm grafting. The Raman spectra in Figure 1B confirm defect formation, with the D-band near 1,350 cm^{-1} assigned to sp^3-hybridized carbon and the G-band near 1,588 cm^{-1} representing sp^2-hybridized carbon[31]. Also, the I_D/I_G (D/G intensity ratio) value increased from 1.27 in pristine CNTs to 1.41 in PAM-g-CNTs, indicating sulfate radicals effectively induce functional sites on the CNT surface, thereby enabling the covalent attachment of AAm monomers at these reactive sites[32].

To confirm the successful synthesis of PAM-g-CNTs, XPS, TGA, and TEM-EELS were conducted. In the XPS N 1s spectrum of PAM-g-CNTs, a distinct peak at 399.5 eV corresponding to the N-C=O bond was observed, providing clear evidence of successful PAM grafting onto the CNT surface [Figure 1C]. TGA analysis ranging from room temperature to 800 °C revealed that grafted PAM accounts for approximately 3.9% of the total weight of PAM-g-CNTs [Figure 1D][33]. Additionally, TEM-EELS mapping displayed a uniform distribution of nitrogen atoms across the PAM-g-CNT surfaces, suggesting that PAM chains were consistently grafted onto the CNT [Figure 1E][34].

Enhanced dispersibility of PAM-g-CNTs

In manufacturing Si-based electrodes, uniform CNT dispersion in the aqueous slurry is critical for fabricating a homogeneous mixture, directly influencing the electrode's quality and uniformity. To evaluate the dispersibility of PAM-g-CNTs, equal amounts of PAM-g-CNTs and unmodified CNTs were dispersed in DI water [Figure 2A]. Optical images were taken right after the sonication and subsequently one month later. Once dispersed, pristine CNTs are rapidly aggregated and precipitated, with continued precipitation noted one month later. In contrast, PAM-g-CNTs were homogenously dispersed and remained suspended stably throughout a long-term period of one month. The marked improvement in dispersibility of PAM-g-CNTs is attributed to their increased hydrophilicity, which strengthens interactions between the CNT surface and surrounding water molecules, thereby effectively preventing aggregation[35]. Additionally, the PAM chains introduce steric hindrance, acting as a physical barrier that inhibits re-aggregation and supports the consistent dispersion of the PAM-g-CNTs[36].

The presence of hydrophilic PAM chains also promotes the interaction of PAM-g-CNTs with Si surfaces in the electrodes. PAM-g-CNTs can engage in hydrogen bonding with hydroxyl groups (-OH) on the Si surface and with polar functional groups in aqueous binders such as PAA. When analyzing the viscosity of the Si electrode slurry as a function of shear rate, the slurry containing PAM-g-CNTs displayed a relatively higher viscosity in the low shear rate regime than that containing unmodified CNTs [Supplementary Figure 2]. This means that while CNTs rely on van der Waals forces between components, which would make the slurry less dispersible over time, PAM-g-CNTs interact with solvent molecules, Si particles, and binders in the slurry through hydrogen bonding, allowing the slurry to remain dispersible over time. This interaction was further verified through Raman analysis of PAA binder films with conductive agents labeled CNT@PAA and PAM-g-CNT@PAA, prepared by mixing each conductive material with PAA in a 1:1 weight ratio [Supplementary Figure 3]. In the PAM-g-CNT@PAA spectra, an upward shift in the G-band peak from 1,588 cm^{-1} to 1,602 cm^{-1} was observed compared to PAM-g-CNTs. G-band shift is closely related to the withdrawal of π electrons from the CNTs, which is well-known to occur due to intermolecular hydrogen bonding within the material. Thus, the observed upshift in the G-band suggests the presence of hydrogen bonding between PAM-g-CNTs and PAA[37].

Homogeneously dispersed PAM-g-CNTs in the slurry form a coherent structure throughout the electrode, as confirmed by micro-computed tomography (micro-CT) and 3D laser microscopy analysis at the electrode level. Micro-CT images demonstrate that unmodified CNTs were agglomerated, while the PAM-g-CNTs were evenly distributed without such aggregation [Figure 2B and C]. Likewise, 3D laser microscope images showing electrode surface roughness reveal that CNT-based electrodes displayed considerable thickness deviations ranging from -2 μm to 40 μm due to a serious agglomeration of CNTs, which can lead to the uneven current distribution, causing localized hot spots and reducing the battery efficiency [Figure 2D]. In contrast, the PAM-g-CNT-based electrode [Figure 2E] exhibited minimal height variation (-2 μm to 3 μm). Scanning electron microscopy (SEM) images further show consistently dispersed Si and the conductive agent at the electrode with PAM-g-CNT [Supplementary Figure 4A and B], indicating that PAM-g-CNTs promote a uniform network for electron flow across the electrode, supporting stable

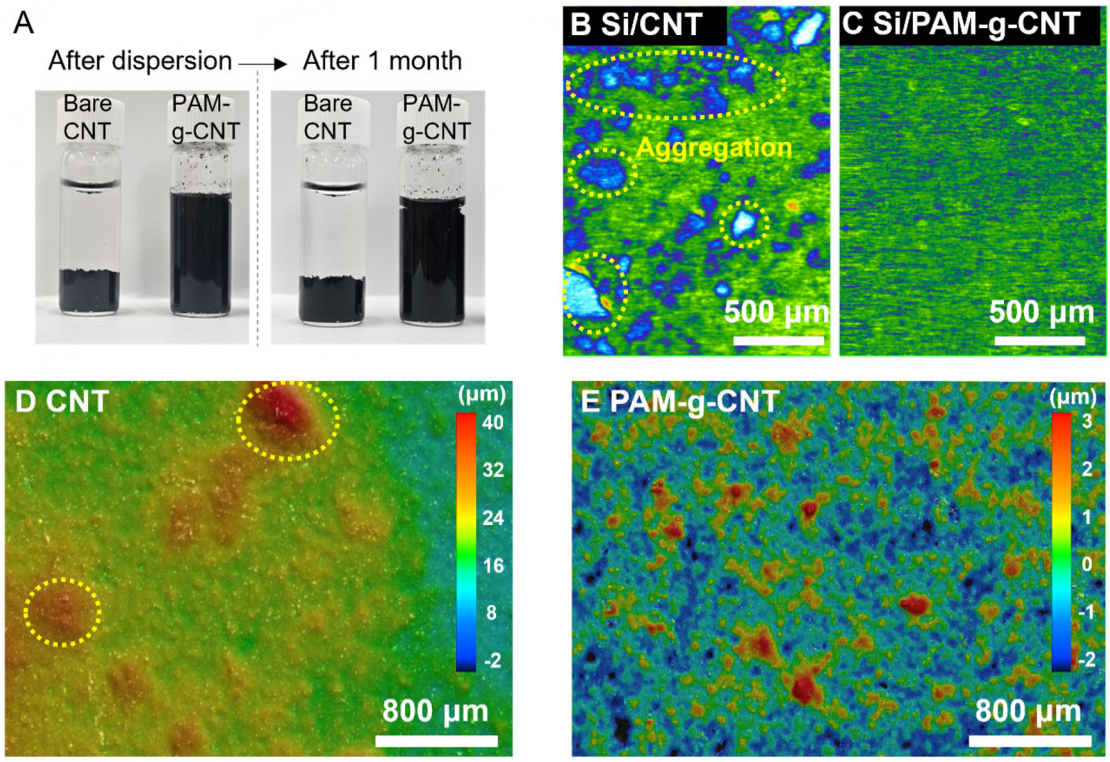

Figure 2. Dispersibility of Si and CNTs. (A) Optical images of CNTs and PAM-g-CNTs dispersed in DI water. Micro-CT images of Si mixture with (B) CNTs and (C) PAM-g-CNTs; 3D laser scanned images of Si electrodes with (D) CNTs and (E) PAM-g-CNTs. CNTs: Carbon nanotubes; PAM-g-CNTs: polyacrylamide-grafted CNTs; DI: deionized; 3D: three-dimensional.

battery performance, safety, and longevity.

Characterization of Si electrodes with different conductive agents

CV analysis was conducted on half cells using Si electrodes containing CNTs or PAM-g-CNTs to assess the electrochemical behavior [Supplementary Figure 5]. In the CV curves, the Si@PAM-g-CNT/Li cell demonstrated a more rapid and reversible redox reaction than the Si@CNT/Li cell, as evidenced by higher peak currents at the cathodic peaks (0.20 V, 0.01 V) and anodic peaks (0.37 V and 0.53 V)[38]. The electrochemical kinetics were further investigated using a galvanostatic intermittent titration technique (GITT) to examine Li-ion diffusion across varying lithiation states [Supplementary Figure 6]. The GITT test applied a 0.3 C charge/discharge rate, followed by a 10-minute pulse and a 40-minute rest period[39]. A higher Li^+ diffusion coefficient of 2.91×10^{-9} cm^2 s^{-1} was observed in the PAM-g-CNT electrode, compared to 1.63×10^{-9} cm^2 s^{-1} for the CNT electrode [Figure 3A and B]. The even distribution of PAM-g-CNTs creates a uniform lithium-ion pathway that facilitates Li^+ movement, thereby reducing charge transfer resistance (R_{ct}) and supporting stable electrochemical performance at high current densities.

The intermolecular interaction between PAM-g-CNTs and electrode components strengthens the mechanical cohesion and durability of the electrode, as confirmed by the SAICAS [Figure 3C]. In this analysis, electrodes were precisely cut at an angle to compare shear strength via horizontal force measurement[40]. For the electrodes containing PAM-g-CNT, the maximum horizontal force reached 0.174 N, nearly double the 0.081 N found in the bare CNT electrodes, with average force values of 0.104 N for PAM-g-CNT compared to 0.056 N for bare CNTs.

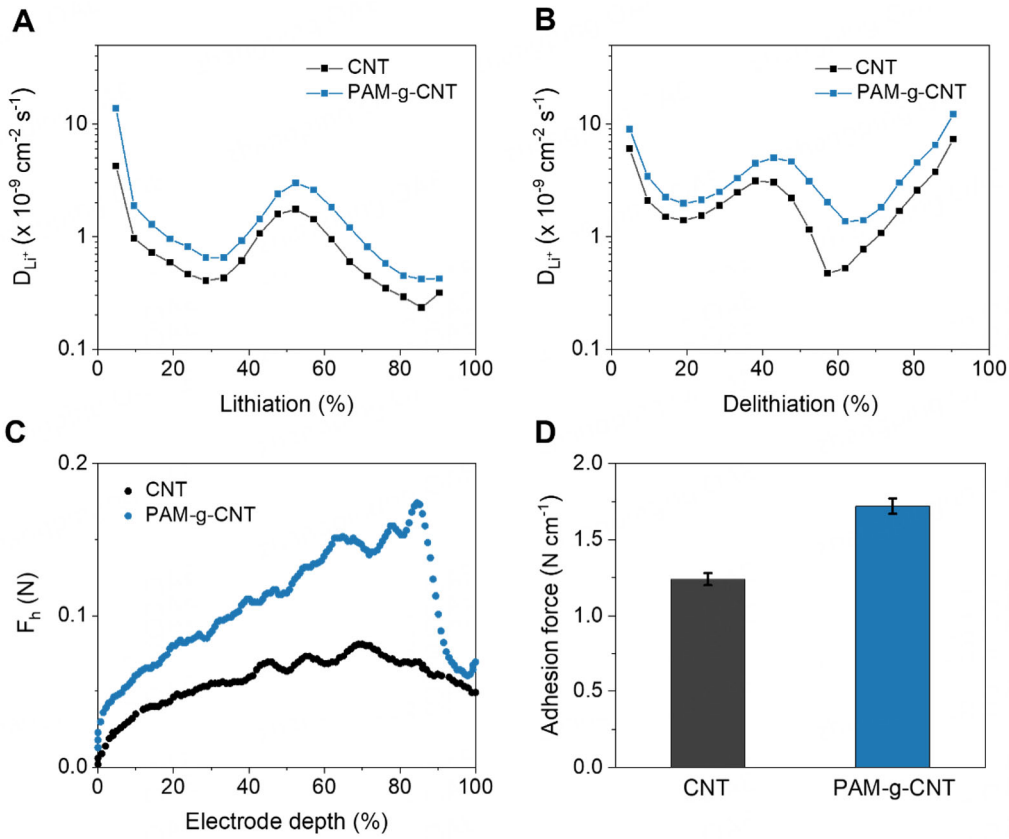

Figure 3. Characterization of Si anodes with CNTs and PAM-g-CNTs. Li^+ diffusion coefficients, which were calculated from GITT during (A) the lithiation and (B) delithiation; (C) SAICAS horizontal force profiles of the electrode; (D) Average adhesion force based on peel-off test results. CNTs: Carbon nanotubes; PAM-g-CNTs: polyacrylamide-grafted CNTs; GITT: galvanostatic intermittent titration technique; SAICAS: surface and interfacial characterization analysis system.

A 180° peel-off test further supported the adhesive properties of Si electrodes with CNTs and PAM-g-CNTs. The PAM-g-CNT electrode demonstrated an average peel strength of 1.74 N cm^{-1}, exceeding the 1.21 N cm^{-1} seen in bare CNT electrodes [Figure 3D and Supplementary Figure 7A]. Additionally, less delamination of active material was observed in the PAM-g-CNT electrode after the peel-off test [Supplementary Figure 7B and C]. These results validate the mechanical resilience and adhesive strength of PAM-g-CNT electrodes, suggesting that PAM-g-CNTs can mitigate structural degradation within the electrode and support stable long-term cycling performance.

Electrochemical performance of Si anodes

The Si/Li coin half-cells were fabricated with Si anodes using SP, CNTs, and PAM-g-CNTs as conductive materials, with Li foil as the counter electrode. Here, CNTs or PAM-g-CNTs were mixed with SP in a weight ratio of 4:1 rather than being used independently. Si mass loading was 0.7-0.8 mg cm^{-2}.

Figure 4A displays the first discharge/charge profiles of the Si/Li half-cells. The SP/PAM-g-CNT 4:1 electrode delivered the highest capacity of 3,415 mA h g^{-1}, outperforming both the SP electrode (2,936 mA h g^{-1}) and the SP/CNT 4:1 electrode (2,669 mA h g^{-1}). Additionally, it showed the lowest overpotential, consistent with the findings from EIS conducted on the 1 cycled cells [Supplementary Figure 8]. Figure 4B presents the R_{ct} and solid electrolyte interphase (SEI) layer resistance (R_{SEI}) values from EIS spectra, where R_{ct} is notably lower for SP/PAM-g-CNT 4:1 (32.53 Ω) than for SP (129.3 Ω) and SP/CNT 4:1

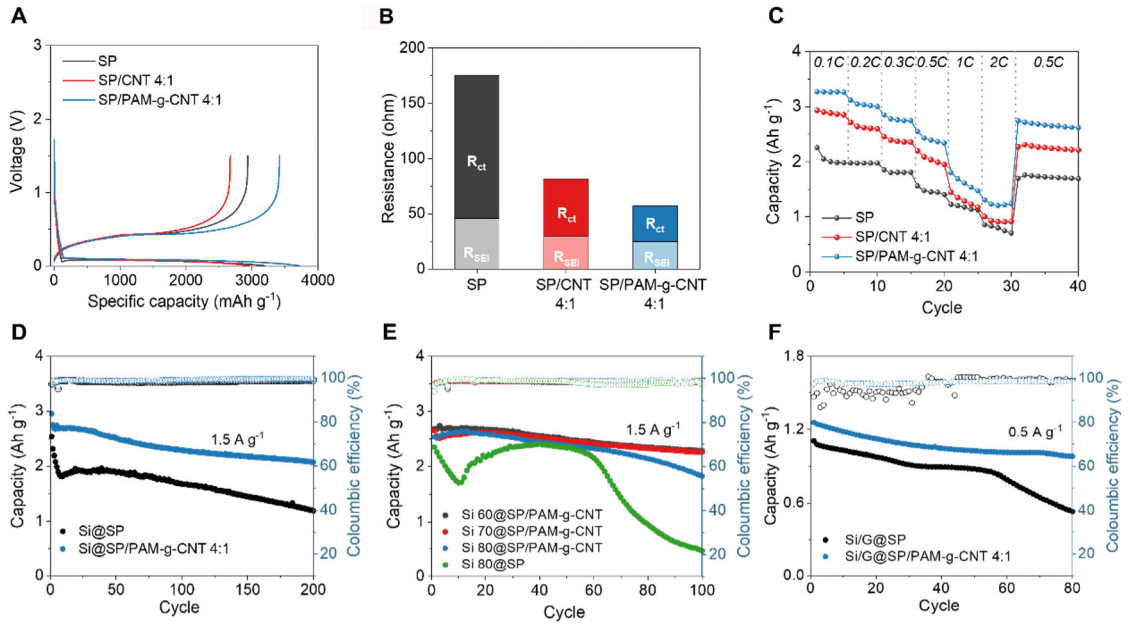

Figure 4. Electrochemical performance of Si-based electrodes. (A) Voltage profiles of formation cycle; (B) Comparison of polarization resistance (R_{SEI} and R_{ct}) after one cycle; (C) The rate capability of Si anodes containing different conductive materials; (D) Long-term stability of Si anodes with SP and SP/PAM-g-CNT 4:1; (E) Cycling performance of Si anodes with varying active material content; (F) Cycling performance of Si/Gr blended anodes. SP: Super P; CNTs: carbon nanotubes; PAM-g-CNTs: polyacrylamide-grafted CNTs.

(51.77 Ω), while R_{SEI} values show less disparity. The prominent reduction in R_{ct} points to a fast electron transfer rate of SP/PAM-g-CNT 4:1, attributed to the well-dispersed, long-strand structure of PAM-g-CNTs which establish broad contact with Si particles and foster interconnected pathways for both electron and ion transport in the electrode[41].

To compare rate capabilities, Si anodes with different conductive agents were assessed by varying the current density from 0.1 C to 2.0 C [Figure 4C]. Under high current conditions of 6 A g^{-1}, SP/PAM-g-CNT 4:1 achieved a superior capacity of 1,239.6 mA h g^{-1} compared to SP (708.2 mA h g^{-1}) and SP/CNT 4:1 (918.3 mA h g^{-1}). When the current density returned to 0.3 A g^{-1}, SP/PAM-g-CNT 4:1 recovered a 2,740.0 mA h g^{-1}. Beyond rate performance, PAM-g-CNT electrodes also demonstrated superior stability in long-term cycling. As shown in Figure 4D, SP electrodes held only 62.9% of their initial capacity after 200 cycles with a continuous capacity loss. However, PAM-g-CNT electrodes retained 78.9% of their initial capacity, underscoring their robust cycle stability.

Achieving a high active material content in Si anodes presents challenges in maintaining adhesive strength within the conductive network. PAM-g-CNTs play a dual role by enhancing conductivity and strengthening adhesion between active materials, thus preserving electrode structure even with a lower ratio of conductive material to the binder. To verify this, the cycle stability of Si anodes prepared with active material ratios of 60% (Si 60@PAM-g-CNTs), 70% (Si 70@PAM-g-CNTs), and 80% (Si 80@PAM-g-CNTs) was evaluated [Figure 4E]. Both Si 60@PAM-g-CNT and Si 70@PAM-g-CNT retained capacities over 80%, respectively. Notably, when the Si content reached 80%, Si 80@PAM-g-CNT maintained stable cycling up to 100 cycles, whereas Si 80@SP suffered a rapid degradation after 50 cycles. This difference stems from the lack of structural strength in SP and its weak bonding with both Si and the binder, which makes low binder and conductive agent content particularly detrimental. SP-containing electrodes become fragile, cracking more easily and quickly losing electrical contact as they expand and contract, which leads to blocked ion channels

and declining capacity[21]. Meanwhile, PAM-g-CNTs, characterized by their linear stranded structure and strong binding ability, are well dispersed within the electrode and firmly attached to the Si particles. They maintain the electron-conducting network and hold the bonds between the active materials during repeated cycling[28]. As a result, even with limited amounts of binder and conductive agent, PAM-g-CNTs significantly enhance performance stability at high Si content. Electrochemical evaluation of Si/Gr (3:7) anodes further showed that Si/Gr@SP/PAM-g-CNT (4:1)/Li half-cell demonstrated improved cycle stability over Si/Gr@SP, which suffered notable capacity fading after 60 cycles [Figure 4F]. To investigate the impact of PAM-g-CNT dispersion on a larger electrode area, a 65 mA h pouch cell using a SiO_x/Gr anode (5.4 cm × 6.4 cm) paired with a $Li[Ni_{0.8}Co_{0.1}Mn_{0.1}]O_2$ (NCM811) cathode was assembled [Supplementary Figure 9]. The well-dispersed PAM-g-CNTs over the extended area prevented current from concentrating in localized regions, supporting 81.6% capacity retention in the pouch cell after 200 cycles.

Dispersants are commonly employed to achieve a homogeneous dispersion of CNTs while minimizing surface damage. PVP is a widely used dispersant for CNTs. However, the PAM-g-CNTs with improved dispersibility would allow them to achieve effects similar to those of dispersants without adding agents. PVP promotes CNT dispersion through physical steric hindrance by adhering to the CNT surface; however, its reliance on weaker physical interactions limits the long-term stability of PVP-CNT. In contrast, PAM-g-CNT achieves high dispersibility by covalently grafting PAM chains onto the CNT surface, resulting in a more resilient and structurally stable structure. Additionally, the much stronger hydrophilicity of PAM enables effective interactions with polar solvents, Si particles, and binders, thereby fostering strong intercomponent cohesion. Consequently, unlike PVP, PAM-g-CNTs fortify the electrode by forming stable chemical bonds, establishing reliable conductive networks, and enhancing mechanical durability, making it an optimal choice for high-performance Si-based LIBs [Supplementary Figure 10].

Post-mortem analysis of Si electrodes

SEM analysis of the cycled Si anodes compared the electrode morphology. Following 50 cycles, SEM images reveal severe surface damage in SP and SP/CNT electrodes, with extensive microcracks allowing electrolyte penetration that triggers detrimental side reactions and leads to electrode swelling (156% for SP and 125% for SP/CNT) [Figure 5A and B]. On the other hand, SP/PAM-g-CNT electrodes retained an intact surface and underwent minimal thickness increase (69%) [Figure 5C]. The strong interaction with Si based on the hydrogen bonding of PAM-g-CNTs confirmed that electrodes with PAM-g-CNT have mechanical resilience and strong adhesion. The electrode's improved mechanical properties allowed SP/PAM-g-CNTs 4:1 to maintain structural integrity despite repeated volume changes of Si during cycling, leading to excellent long-term cell performance.

CONCLUSIONS

In summary, CNTs were successfully functionalized with PAM through radical polymerization, substantially improving dispersibility and adhesion within Si anodes. PAM-g-CNTs address the aggregation issues associated with hydrophobic CNTs by introducing hydrophilic PAM chains, which create a physical barrier between CNTs and interact with aqueous solvents. Notably, PAM-g-CNTs remained well-dispersed in water for over a month, enabling homogeneous electrode slurries that yielded high-quality electrodes, as confirmed by micro-CT and 3D laser microscopy. Beyond its role as a conductive agent, PAM-g-CNTs engage in hydrogen bonding with other electrode components, strengthening intercomponent binding. Consequently, Si anodes with PAM-g-CNTs demonstrated 1.5 times stronger adhesion than those with bare CNTs, improving electrode durability during cycling. Furthermore, Si@PAM-g-CNT anodes prepared with a high active material ratio (80%) minimizing the conductive material and binder content maintained stable cycling for up to 100 cycles, while Si 80@SP anodes degraded rapidly after 50 cycles, benefiting from the

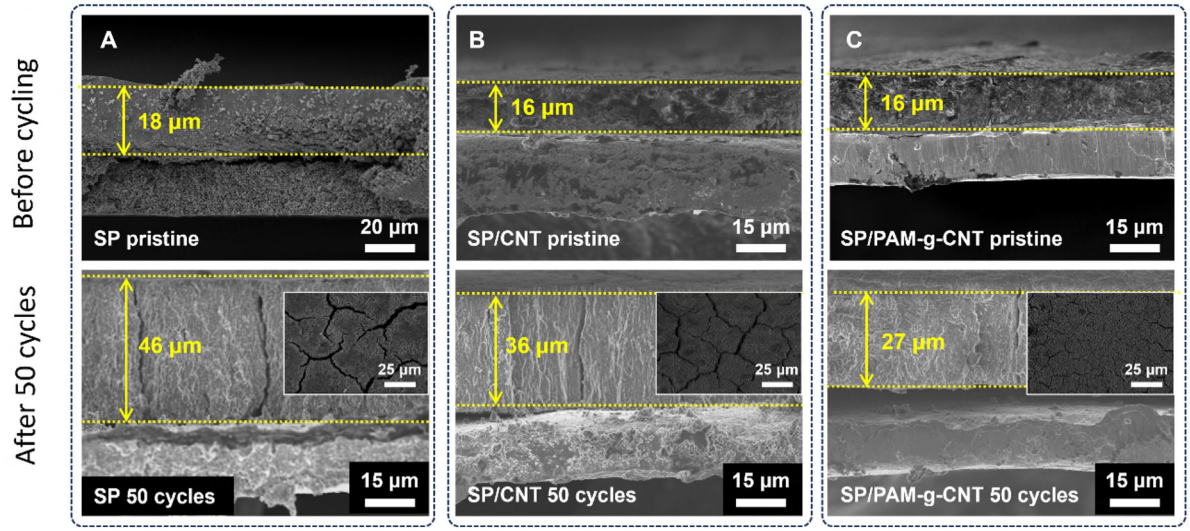

Figure 5. Cross-sectional SEM images of Si anodes with (A) SP; (B) SP/CNT; and (C) SP/PAM-g-CNT at the pristine state and after 50 cycles (Inset: Top-view SEM images of Si electrode surface after 50 cycles). SP: Super P; CNTs: carbon nanotubes; PAM-g-CNTs: polyacrylamide-grafted CNTs; SEM: scanning electron microscopy.

reduced R_{ct} and a well-preserved continuous electron conduction path. The bifunctional CNT modification with hydrophilic polymers offers a promising strategy for high-energy-density anodes, balancing electrical conductivity with structural durability.

DECLARATIONS

Acknowledgments

We thank Junhyeok Noh from Prof. Hee Chul Choi's lab for assistance with the Raman spectroscopy analysis.

Authors' contributions

Manuscript writing, data curation, formal analysis, investigation: Kim,Y.; Nam, S.
Resources and methodology: Jeon, Y.; Han, D. Y.
Conceptualization: Kim, Y.; Jung, J.
Supervision, project administration, funding acquisition: Park, S.
All authors revised the manuscript.

Availability of data and materials

Some results of supporting the study are presented in the Supplementary Materials. Other raw data supporting this study's findings are available from the corresponding author upon reasonable request.

Financial support and sponsorship

This work was supported by the National Research Foundation of Korea (NRF) funded by the Ministry of Science and ICT (2023R1A2C2003939) and the Korea Institute for Advancement of Technology (RS-2024-00419413). Additionally, the results are from a study under the "Leaders in Industry-University Cooperation 3.0" Project, supported by the Ministry of Education and National Research Foundation of Korea.

Conflicts of interest

All authors declared that there are no conflicts of interest.

Ethical approval and consent to participate

Not applicable.

Consent for publication

Not applicable.

Copyright

REFERENCES

1. Feng, K.; Li, M.; Liu, W.; et al. Silicon-based anodes for lithium-ion batteries: from fundamentals to practical applications. *Small* **2018**, *14*, 1702737. DOI
2. Li, P.; Zhao, G.; Zheng, X.; et al. Recent progress on silicon-based anode materials for practical lithium-ion battery applications. *Energy. Storage. Mater.* **2018**, *15*, 422-46. DOI
3. Guo, J.; Dong, D.; Wang, J.; et al. Silicon-based lithium ion battery systems: state-of-the-art from half and full cell viewpoint. *Adv. Funct. Mater.* **2021**, *31*, 2102546. DOI
4. Ko, M.; Chae, S.; Cho, J. Challenges in accommodating volume change of Si anodes for Li-ion batteries. *ChemElectroChem* **2015**, *2*, 1645-51. DOI PubMed PMC
5. McDowell, M. T.; Lee, S. W.; Nix, W. D.; Cui, Y. 25th anniversary article: understanding the lithiation of silicon and other alloying anodes for lithium-ion batteries. *Adv. Mater.* **2013**, *25*, 4966-85. DOI PubMed
6. Yang, Y.; Yuan, W.; Kang, W.; et al. Silicon-nanoparticle-based composites for advanced lithium-ion battery anodes. *Nanoscale* **2020**, *12*, 7461-84. DOI
7. Yang, Y.; Wu, S.; Zhang, Y.; et al. Towards efficient binders for silicon based lithium-ion battery anodes. *Chem. Eng. J.* **2021**, *406*, 126807. DOI
8. Deng, L.; Zheng, Y.; Zheng, X.; et al. Design criteria for silicon-based anode binders in half and full cells. *Adv. Energy. Mater.* **2022**, *12*, 2200850. DOI
9. Tang, J.; Zhou, J.; Duan, X.; Yang, Y.; Dai, X.; Wu, F. Constructing the bonding between conductive agents and active materials/binders stabilizes silicon anode in lithium-ion batteries. *J. Energy. Chem.* **2023**, *80*, 23-31. DOI
10. Huang, L.; You, Y.; Liu, M.; et al. Nanoscale precision welding-enabled quasi-3D conductive carbon blacks for fast-charging and long-lasting secondary batteries. *Carbon* **2024**, *230*, 119688. DOI
11. Kim, D. S.; Lee, J. U.; Kim, S. H.; Hong, J. Electrochemically exfoliated graphite as a highly efficient conductive additive for an anode in lithium□ion batteries. *Battery. Energy.* **2023**, *2*, 20230012. DOI
12. Weng, W.; Sun, Q.; Zhang, Y.; et al. Winding aligned carbon nanotube composite yarns into coaxial fiber full batteries with high performances. *Nano. Lett.* **2014**, *14*, 3432-8. DOI
13. Ren, J.; Li, L.; Chen, C.; et al. Twisting carbon nanotube fibers for both wire-shaped micro-supercapacitor and micro-battery. *Adv. Mater.* **2013**, *25*, 1155-9, 1224. DOI
14. Liu, X.; Huang, Z. D.; Oh, S. W.; et al. Carbon nanotube (CNT)-based composites as electrode material for rechargeable Li-ion batteries: a review. *Compos. Sci. Technol.* **2012**, *72*, 121-44. DOI
15. Lee, H.; Kim, H.; Cho, M. S.; Choi, J.; Lee, Y. Fabrication of polypyrrole (PPy)/carbon nanotube (CNT) composite electrode on ceramic fabric for supercapacitor applications. *Electrochim. Acta.* **2011**, *56*, 7460-6. DOI
16. Kang, H. E.; Ko, J.; Song, S. G.; Yoon, Y. S. Recent progress in utilizing carbon nanotubes and graphene to relieve volume expansion and increase electrical conductivity of Si-based composite anodes for lithium-ion batteries. *Carbon* **2024**, *219*, 118800. DOI
17. Gao, C.; Guo, M.; Liu, Y.; et al. Surface modification methods and mechanisms in carbon nanotubes dispersion. *Carbon* **2023**, *212*, 118133. DOI
18. Avilés, F.; Cauich-rodríguez, J.; Moo-tah, L.; May-pat, A.; Vargas-coronado, R. Evaluation of mild acid oxidation treatments for MWCNT functionalization. *Carbon* **2009**, *47*, 2970-5. DOI
19. Choi, J. H.; Lee, C.; Park, S.; et al. Improved electrochemical performance using well-dispersed carbon nanotubes as conductive additive in the Ni-rich positive electrode of lithium-ion batteries. *Electrochem. Commun.* **2023**, *146*, 107419. DOI
20. Kim, H.; Lim, J. H.; Lee, T.; et al. Ozone-treated carbon nanotube as a conductive agent for dry-processed lithium-ion battery cathode. *ACS. Energy. Lett.* **2023**, *8*, 3460-6. DOI
21. Zhou, J.; Lan, Y.; Zhang, K.; et al. In situ growth of carbon nanotube wrapped Si composites as anodes for high performance lithium ion batteries. *Nanoscale* **2016**, *8*, 4903-7. DOI
22. Feng, X.; Yang, J.; Bie, Y.; Wang, J.; Nuli, Y.; Lu, W. Nano/micro-structured Si/CNT/C composite from nano-SiO_2 for high power

lithium ion batteries. *Nanoscale* **2014**, *6*, 12532-9. DOI PubMed

23. Forney, M. W.; Dileo, R. A.; Raisanen, A.; et al. High performance silicon free-standing anodes fabricated by low-pressure and plasma-enhanced chemical vapor deposition onto carbon nanotube electrodes. *J. Power. Sources.* **2013**, *228*, 270-80. DOI
24. Ding, X.; Wang, H.; Liu, X.; et al. Advanced anodes composed of graphene encapsulated nano-silicon in a carbon nanotube network. *RSC. Adv.* **2017**, *7*, 15694-701. DOI
25. He, Z.; Zhang, C.; Zhu, Z.; Yu, Y.; Zheng, C.; Wei, F. Advances in carbon nanotubes and carbon coatings as conductive networks in silicon□based anodes. *Adv. Funct. Mater.* **2024**, *34*, 2408285. DOI
26. Joo, Y.; Brady, G. J.; Shea, M. J.; et al. Isolation of pristine electronics grade semiconducting carbon nanotubes by switching the rigidity of the wrapping polymer backbone on demand. *ACS. Nano.* **2015**, *9*, 10203-13. DOI
27. Abousalman-Rezvani, Z.; Eskandari, P.; Roghani-Mamaqani, H.; Salami-Kalajahi, M. Functionalization of carbon nanotubes by combination of controlled radical polymerization and "grafting to" method. *Adv. Colloid. Interface. Sci.* **2020**, *278*, 102126. DOI PubMed
28. Deng, L.; Deng, S. S.; Pan, S. Y.; et al. Multivalent amide-hydrogen-bond supramolecular binder enhances the cyclic stability of silicon-based anodes for lithium-ion batteries. *ACS. Appl. Mater. Interfaces.* **2021**, *13*, 22567-76. DOI
29. Zhang, M.; Ning, G.; Xiao, Z. Binder-assisted dispersion of agglomerated carbon nanotubes for efficiently establishing conductive networks in cathodes of Li-ion batteries. *Energy. Technol.* **2020**, *8*, 2000589. DOI
30. Gunavadhi, M.; Maria, L. A.; Chamundeswari, V. N.; Parthasarathy, M. Nanotube-grafted polyacrylamide hydrogels for electrophoretic protein separation. *Electrophoresis* **2012**, *33*, 1271-5. DOI PubMed
31. Ma, H.; Tong, L.; Xu, Z.; Fang, Z. Functionalizing carbon nanotubes by grafting on intumescent flame retardant: nanocomposite synthesis, morphology, rheology, and flammability. *Adv. Funct. Mater.* **2008**, *18*, 414-21. DOI
32. Wang, X.; Ouyang, C.; Dou, S.; Liu, D.; Wang, S. Oxidized carbon nanotubes as an efficient metal-free electrocatalyst for the oxygen reduction reaction. *RSC. Adv.* **2015**, *5*, 41901-4. DOI
33. Li, Z.; Tang, M.; Dai, J.; Wang, T.; Bai, R. Effect of multiwalled carbon nanotube-grafted polymer brushes on the mechanical and swelling properties of polyacrylamide composite hydrogels. *Polymer* **2016**, *85*, 67-76. DOI
34. Xiong, H.; Motchelaho, M. A.; Moyo, M.; Jewell, L. L.; Coville, N. J. Fischer-tropsch synthesis: iron-based catalysts supported on nitrogen-doped carbon nanotubes synthesized by post-doping. *Appl. Catal. A. Gen.* **2014**, *482*, 377-86. DOI
35. Abo-hamad, A.; Hayyan, M.; Alsaadi, M. A.; Mirghani, M. E.; Hashim, M. A. Functionalization of carbon nanotubes using eutectic mixtures: a promising route for enhanced aqueous dispersibility and electrochemical activity. *Chem. Eng. J.* **2017**, *311*, 326-39. DOI
36. Huang, Y. Y.; Terentjev, E. M. Dispersion of carbon nanotubes: mixing, sonication, stabilization, and composite properties. *Polymers* **2012**, *4*, 275-95. DOI
37. Han, J. T.; Kim, S. Y.; Woo, J. S.; Jeong, H. J.; Oh, W.; Lee, G. Hydrogen-bond-driven assembly of thin multiwalled carbon nanotubes. *J. Phys. Chem. C.* **2008**, *112*, 15961-5. DOI
38. Zeng, W.; Wang, L.; Peng, X.; et al. Enhanced ion conductivity in conducting polymer binder for high-performance silicon anodes in advanced lithium-ion batteries. *Adv. Energy. Mater.* **2018**, *8*, 1702314. DOI
39. Weppner, W.; Huggins, R. A. Determination of the kinetic parameters of mixed-conducting electrodes and application to the system Li_3Sb. *J. Electrochem. Soc.* **1977**, *124*, 1569-78. DOI
40. Son, B.; Ryou, M. H.; Choi, J.; et al. Measurement and analysis of adhesion property of lithium-ion battery electrodes with SAICAS. *ACS. Appl. Mater. Interfaces.* **2014**, *6*, 526-31. DOI
41. Zhang, F.; Xia, H.; Wei, T.; Li, H.; Yang, M.; Cao, A. A new universal aqueous conductive binder *via* esterification reinforced electrostatic/H-bonded self-assembly for high areal capacity and stable lithium-ion batteries. *Energy. Environ. Sci.* **2024**, *17*, 238-48. DOI